

pp 191–211. © Royal Aeronautical Society 2019
doi:[10.1017/aer.2018.158](https://doi.org/10.1017/aer.2018.158)

Classification of UAV and bird target in low-altitude airspace with surveillance radar data

W. S. Chen

wishchen@buaa.edu.cn

J. Liu and J. Li

Airport Research Institute
China Academy of Civil Aviation Science and Technology
Beijing
China

ABSTRACT

In order to ensure low-altitude safety, a tracking and recognition method of unmanned aerial vehicle (UAV) and bird targets based on traditional surveillance radar data is proposed. First, several motion models for UAV and flying bird targets are established. Second, the target trajectories are filtered and smoothed with multiple motion models. Third, by calculating the time-domain variance of the model occurrence probability, the model conversion probability of the target is estimated, and then the target type is identified and classified. The effectiveness and robustness of the algorithm is demonstrated by several groups of Monte Carlo simulation experiments, including setting different recognition steps, different model transformation probability, filtering and smoothing algorithm comparison. The algorithm is also successfully applied on the ground-truth radar data collected by the low-altitude surveillance radar at airport and coastal environments, where the targets of UAVs and flying birds could be tracked and recognised.

Keywords: Classification; UAV; Bird; Target; Radar

Received 8 October 2018; revised 2 November 2018; accepted 8 November 2018.

NOMENCLATURE

LSS	slow speed small
RMSE	root mean square error
ROC	receiver operator characteristic
UAV	unmanned aerial vehicle

1.0 INTRODUCTION

In recent years, with the rapid development of the unmanned aerial vehicle (UAV) industry, the interference incidents to civil aviation by UAV frequently occur at various airports around the world⁽¹⁾. The potential safety hazards caused by the illegal flight of UAVs have sounded an alarm for the low-altitude airspace protection of airports, frontiers and important sensitive areas, which has aroused great public concern. According to the communication between the target and the detection equipment, the low-altitude, slow speed small (LSS) target represented by UAV can be divided into ‘co-operation’ and ‘non-co-operation’. For co-operative UAV, its flight information can be real-time accessed to the UAV Cloud management system, and the regulatory authorities will inquire and record the UAV mistakenly entering the corresponding area⁽²⁾. Co-operative surveillance technology can cover more than 95% of the consumer UAV, and the remaining less than 5% of the non-co-operative UAV is the focus and difficulty of low-altitude defence.

At present, typical non-co-operative UAV target detection technologies include photoelectric, radio detection, acoustics, radar and so on, each of which has its own advantages and short comings^(3–9). Among them, radio detection technology can effectively detect the UAV operator but cannot effectively find the ‘silent’ UAV without transmitting radio signals. Although photoelectric detection has advantages in target recognition, it is easy to be interfered by ambient light and the detection range is limited. Audio detection technology is susceptible to noise and clutter, which has a good effect on large UAVs, but it is difficult to detect small and medium-sized UAVs in strong background noise environment. Generally speaking, as the main means of target detection and surveillance, radar is widely used in the fields of defence and public security, such as air and sea target surveillance and early warning. Although the traditional radar has the problem of insufficient detection efficiency for LSS targets, radar is still an important means of air target detection⁽¹⁰⁾.

In the low-altitude environment, flying birds are the main LSS targets besides UAVs. In the process of UAVs and flying birds target detection, it is necessary to classify and identify them. In general, radar can only obtain the amplitude, position, speed information of the target as the single detection means, which is difficult to effectively classify and identify the target. At present, the typical low-altitude surveillance system uses optoelectronic technology as a supplement to the radar system, which identifies and confirms the target after the radar finds it⁽¹¹⁾. However, the cost of such systems is high, and the synchronisation of radar and optoelectronic equipment is difficult due to the limited view field of optoelectronic equipment and the need to adjust the focal length when detecting targets at different distances. A large number of researchers have identified UAVs and flying birds by extracting the micro-Doppler characteristics of the target, but this kind of research is only applicable to metal-rotor UAVs with strong radar echo^(12–16). There is no relevant report on the recognition of light and small UAVs with weak echo, such as the Phantom series of DJI.

Aiming at the above problems, a method is proposed for the classification and recognition of low-altitude non-co-operative UAV and flying bird targets based on motion model, using the echo information obtained by conventional mechanical scanning radar to fully analyse the difference between UAV and flying bird targets. The remaining of this paper is organised as follows. In Section 2, the proposed scheme and modelling method is introduced. Then, some analysis results for the simulated and real data are provided, respectively, in Sections 3 and 4. Some conclusions close the paper in Section 5.

2.0 MODELLING AND ANALYSIS

The scattering cross section, flying speed and flying height of low-altitude flying bird target are close to those of light and small UAV, so the existing low-altitude surveillance radar is difficult to distinguish them. In this section, the basic scheme flow of classification and recognition algorithm of light and small UAV and flying bird based on motion model is given, and then the establishment of motion model and the method of feature extraction are described in detail.

2.1 Scheme design

In this algorithm, four steps are adopted: target tracking with multiple models, target smoothing, model probability estimation and feature extraction of target models. Finally, target features such as target motion model conversion frequency are extracted to distinguish light and small UAV targets from flying birds. The algorithm flow chart is shown in Fig. 1. Existing target tracking methods estimate target state information by establishing target motion model and modify target state by using measurement information, whose purpose is to improve tracking accuracy and approximate the real moving state of target. The goal of this method is not to improve the tracking accuracy but to realise the recognition and classification of the target, which is an extension application of the existing target tracking algorithm.

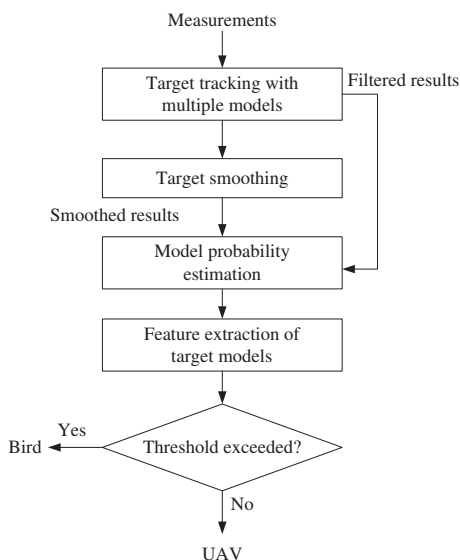


Figure 1. Classification scheme for unmanned aerial vehicle (UAV) and flying bird targets.

2.2 Target tracking with multiple models

In each time step, the initial conditions are obtained for certain model-matched filter by mixing the state estimates produced by all filters from the previous time step under the assumption that this particular model is the right model at current time step. Then standard Kalman filtering is performed for each model, and after that we compute a weighted combination of updated state estimates produced by all the filters yielding a final estimate for the state and covariance of the Gaussian density in that particular time step. The weights are chosen according to the probabilities of the models, which are computed in filtering step of the algorithm.

The mixing probabilities $\mu_k^{i|j}$ for each model M^i and M^j are calculated as

$$\bar{c}_j = \sum_{i=1}^n P_{ij} \mu_{k-1}^i, \tag{1}$$

$$\mu_k^{i|j} = \frac{1}{\bar{c}_j} P_{ij} \mu_{k-1}^i, \tag{2}$$

where μ_{k-1}^i is the probability of model M^i in the time step $k-1$ and \bar{c}_j a normalisation factor.

Now we can compute the mixed mean and covariance for each filter as

$$\mathbf{m}_{k-1}^{0j} = \sum_{i=1}^n \mu_k^{i|j} \mathbf{m}_{k-1}^i, \tag{3}$$

$$\mathbf{P}_{k-1}^{0j} = \sum_{i=1}^n \mu_k^{i|j} \times \left\{ \mathbf{P}_{k-1}^i + \left[\mathbf{m}_{k-1}^i - \mathbf{m}_{k-1}^{0j} \right] \left[\mathbf{m}_{k-1}^i - \mathbf{m}_{k-1}^{0j} \right]^T \right\}, \tag{4}$$

where \mathbf{m}_{k-1}^i and \mathbf{P}_{k-1}^i are the updated mean and the covariance for model i at time step $k-1$.

In the filtering step, for each model M^i , the filtering is done as

$$\left[\mathbf{m}_k^{-,i}, \mathbf{P}_k^{-,i} \right] = \text{KF}_p(\mathbf{m}_{k-1}^{0j}, \mathbf{P}_{k-1}^{0j}, \mathbf{A}_{k-1}^i, \mathbf{Q}_{k-1}^i), \tag{5}$$

$$\left[\mathbf{m}_k^i, \mathbf{P}_k^i \right] = \text{KF}_u(\mathbf{m}_k^{-,i}, \mathbf{P}_k^{-,i}, \mathbf{y}_k, \mathbf{H}_k^i, \mathbf{R}_k^i), \tag{6}$$

where the prediction and update steps of the standard Kalman filter are denoted with $\text{KF}_p(\cdot)$ and $\text{KF}_u(\cdot)$, correspondingly. In addition to mean and covariance, the likelihood of the measurement is also computed for each filter as

$$\Lambda_k^i = N(\mathbf{v}_k^i; 0, \mathbf{S}_k^i), \tag{7}$$

where \mathbf{v}_k^i is the measurement residual and \mathbf{S}_k^i is covariance for model M^i in the KF update step.

The probabilities of each model M^i at time step k are calculated as

$$c = \sum_{i=1}^n \Lambda_k^i \bar{c}_i, \tag{8}$$

$$\mu_k^i = \frac{1}{c} \Lambda_k^i \bar{c}_i, \tag{9}$$

where c is a normalising factor.

Finally, the combined estimate for the state mean and covariance are computed as

$$\mathbf{m}_k = \sum_{i=1}^n \mu_k^i \mathbf{m}_k^i \tag{10}$$

$$\mathbf{P}_k = \sum_{i=1}^n \mu_k^i \times \{ \mathbf{P}_k^i + [\mathbf{m}_k^i - \mathbf{m}_k][\mathbf{m}_k^i - \mathbf{m}_k]^T \} \tag{11}$$

2.3 Target smoothing

It is useful to smooth the state estimates by using all the obtained measurements. Since the optimal fixed-interval smoothing with n models and N measurements requires running n^N smoothers, we must resort to suboptimal approaches. One possibility is to combine the estimates of two filters, one running forwards and the other backwards in time. This approach is restricted to systems having invertible state dynamics, which is always the case for discretised continuous-time systems.

First we shall review the equations for the filter running backwards in time and then the actual smoothing equations combining the estimates of the two filters.

Our aim is now to compute the backward filtering density $p(\mathbf{x}_k | \mathbf{y}_{k:N})$ for each time step, which is expressed as a sum of model conditioned densities

$$p(\mathbf{x}_k | \mathbf{y}_{k:N}) = \sum_{j=1}^n \mu_k^{b,j} p(\mathbf{x}_k^j | \mathbf{y}_{k:N}), \tag{12}$$

where $\mu_k^{b,j}$ is the backward-time filtered model probability of M_k^j . In the last time step N , this is the same as the forward filter’s model probability, that is, $\mu_N^{b,j} = \mu_N^j$. Assuming the model conditioned densities $p(\mathbf{x}_k^j | \mathbf{y}_{k:N})$ are Gaussians the backward density in Fig (12) is a mixture of Gaussians, which is now going to be approximated with a single Gaussian via moment matching.

The model conditioned backward-filtering densities can be expressed as

$$p(\mathbf{x}_k^j | \mathbf{y}_{k:N}) = \frac{1}{c} p(\mathbf{y}_{k:N} | \mathbf{x}_k^j) p(\mathbf{x}_k^j | \mathbf{y}_{k+1:N}), \tag{13}$$

where c is the normalising constant, $p(\mathbf{y}_{k:N} | \mathbf{x}_k^j)$ is the model-conditioned measurement likelihood and $p(\mathbf{x}_k^j | \mathbf{y}_{k+1:N})$ is the model-conditioned density of the state given the future measurements. The latter density is expressed as

$$p(\mathbf{x}_k^j | \mathbf{y}_{k+1:N}) = \sum_{i=1}^n \mu_{k+1}^{b,i|j} p(\mathbf{x}_k^j | M_{k+1}^i, \mathbf{y}_{k+1:N}), \tag{14}$$

where $\mu_{k+1}^{b,i|j}$ is the conditional model probability computed as

$$\mu_{k+1}^{b,i|j} = P\{M_{k+1}^i | M_k^j, \mathbf{y}_{k+1:N}\} = \frac{1}{a_j} p_{i,j}^{b,k} \mu_{k+1}^{b,i}, \tag{15}$$

where a_j is a normalisation constant given by

$$a_j = \sum_{i=1}^n p_{i,j}^{b,k} \mu_{k+1}^{b,i} \tag{16}$$

The backward-time transition probabilities of switching from model M_{k+1}^i to model M_k^j in Figs (15) and (16) are defined as $p_{i,j}^{b,k} = P\{M_k^j | M_{k+1}^i\}$. The prior model probabilities can be computed off-line recursively for each time step k as

$$P\{M_k^j\} = \sum_{i=1}^n P\{M_k^j \mid M_{k-1}^i\} P\{M_{k-1}^i\}, \quad \dots(17)$$

$$= \sum_{i=1}^n p_{ij} P\{M_{k-1}^i\}, \quad \dots(18)$$

and using these we can compute $p_{i,j}^{b,k}$ as

$$p_{i,j}^{b,k} = \frac{1}{b_i} p_{ji} P\{M_k^j\}, \quad \dots(19)$$

where b_i is the normalising constant

$$b_i = \sum_{j=1}^n p_{ji} P\{M_k^j\} \quad \dots(20)$$

The density $p(x_k^j \mid M_{k+1}^i, y_{k+1:N}^N)$ is now approximated with a Gaussian $N(\mathbf{x}_k \mid \mathbf{m}_{k|k+1}^{b,i}, \mathbf{P}_{k|k+1}^{b,-(i)})$ where the mean and the covariance are given by the Kalman filter prediction step using the inverse of the state transition matrix

$$[\hat{\mathbf{m}}_k^{b,i}, \hat{\mathbf{P}}_k^{b,i}] = \text{KF}_p(\mathbf{m}_{k+1}^{b,i}, \mathbf{P}_{k+1}^{b,i}, (\mathbf{A}_{k+1}^i)^{-1}, \mathbf{Q}_{k+1}^i) \quad \dots(21)$$

The density $p(\mathbf{x}_k^j \mid \mathbf{y}_{k+1:N})$ in (14) is a mixture of Gaussians, and it is now approximated with a single Gaussian as

$$p(\mathbf{x}_k^j \mid \mathbf{y}_{k+1:N}) = N(\mathbf{x}_k^j \mid \hat{\mathbf{m}}_k^{b,0j}, \hat{\mathbf{P}}_k^{b,0j}), \quad \dots(22)$$

where the mixed predicted mean and the covariance are given as

$$\hat{\mathbf{m}}_k^{b,0j} = \sum_{i=1}^n \mu_{k+1}^{b,i|j} \hat{\mathbf{m}}_k^{b,i}, \quad \dots(23)$$

$$\hat{\mathbf{P}}_k^{b,0j} = \sum_{i=1}^n \mu_{k+1}^{b,i|j} \cdot \left[\hat{\mathbf{P}}_k^{b,i} + (\hat{\mathbf{m}}_k^{b,i} - \hat{\mathbf{m}}_k^{b,0j})(\hat{\mathbf{m}}_k^{b,i} - \hat{\mathbf{m}}_k^{b,0j})^T \right] \quad \dots(24)$$

Now, the filtered density $p(\mathbf{x}_k^j \mid \mathbf{y}_{k:N})$ is a Gaussian $N(\mathbf{x}_k \mid \mathbf{m}_k^{b,j}, \mathbf{P}_k^{b,j})$, and solving its mean and covariance corresponds to running the Kalman filter update step as follows:

$$[\mathbf{m}_k^{b,j}, \mathbf{P}_k^{b,j}] = \text{KF}_u(\hat{\mathbf{m}}_k^{b,0j}, \hat{\mathbf{P}}_k^{b,0j}, \mathbf{y}_k, \mathbf{H}_k^j, \mathbf{R}_k^j) \quad \dots(25)$$

The measurement likelihoods for each model are computed as

$$\Lambda_k^{b,i} = N(\mathbf{v}_k^{b,i}; \mathbf{0}, \mathbf{S}_k^{b,i}), \quad \dots(26)$$

where $\mathbf{v}_k^{b,i}$ is the measurement residual and $\mathbf{S}_k^{b,i}$ is covariance for model M^i in the KF update step. With these, we can update the model probabilities for time step k as

$$\mu_k^{b,j} = \frac{1}{a} a_j \Lambda_k^{b,i}, \quad \dots(27)$$

where a is a normalising constant

$$a = \sum_{j=1}^m a_j \Lambda_k^{b,j} \quad \dots(28)$$

Finally, we can form the Gaussian approximation to overall backward filtered distribution as

$$p(\mathbf{x}_k \mid \mathbf{y}_{k:N}) = N(\mathbf{x}_k \mid \mathbf{m}_k^b, \mathbf{P}_k^b), \quad \dots(29)$$

where the mean and the covariance are mixed as

$$\mathbf{m}_k^b = \sum_{j=1}^n \mu_k^{b,j} \mathbf{m}_k^{b,j}, \quad \dots(30)$$

$$\mathbf{P}_k^b = \sum_{j=1}^n \mu_k^{b,j} \left[\mathbf{P}_k^{b,j} + (\mathbf{m}_k^{b,j} - \mathbf{m}_k^b)(\mathbf{m}_k^{b,j} - \mathbf{m}_k^b)^T \right] \quad \dots(31)$$

We can now proceed to evaluate the fixed-interval smoothing distribution

$$p(\mathbf{x}_k \mid \mathbf{y}_{1:N}) = \sum_{j=1}^n \mu_k^{s,j} p(\mathbf{x}_k^j \mid \mathbf{y}_{1:N}), \quad \dots(32)$$

where the smoothed model probabilities are computed as

$$\mu_k^{s,j} = P\{M_k^j \mid \mathbf{y}_{1:N}\}, \quad \dots(33)$$

$$= \frac{1}{d} d_j \mu_k^j, \quad \dots(34)$$

where μ_k^j is the forward-time filtered model probability, the density $d_j = p(\mathbf{y}_{k+1:N} \mid M_k^j, \mathbf{y}_{1:k})$ and d the normalisation constant given by

$$d = \sum_{j=1}^n d_j \mu_k^j \quad \dots(35)$$

The model-conditioned smoothing distributions $p(\mathbf{x}_k^j \mid \mathbf{y}_{1:N})$ in Fig (32) are expressed as mixtures of Gaussians

$$p(\mathbf{x}_k^j \mid \mathbf{y}_{1:N}) = \sum_{i=1}^n \mu_{k+1}^{s,i|j} p(\mathbf{x}^i \mid M_{k+1}^i, \mathbf{y}_{1:n}), \quad \dots(36)$$

where the conditional probability $\mu_{k+1}^{s,i|j}$ is given by

$$\mu_{k+1}^{s,i|j} = P\{M_{k+1}^i \mid M_k^j, \mathbf{y}_{1:n}\}, \tag{37}$$

$$= \frac{1}{d_j} p_{ji} \Lambda_k^{ji}, \tag{38}$$

and the likelihood Λ_k^{ji} by

$$\Lambda_k^{ji} = p(\mathbf{y}_{k+1:N} \mid M_k^j, M_{k+1}^j, \mathbf{y}_{1:k}) \tag{39}$$

We approximate this now as

$$\Lambda_k^{ji} \approx p(\hat{\mathbf{x}}_k^{b,i} \mid M_k^j, M_{k+1}^j, \mathbf{x}_k^j), \tag{40}$$

which means that the future measurements $\mathbf{y}_{k+1:N}$ are replaced with the n model-conditioned backward-time one-step predicted means and covariances $\left\{ \hat{\mathbf{m}}_k^{b,i}, \hat{\mathbf{P}}_k^{b,i} \right\}_{r=1}^n$, and $\mathbf{y}_{1:k}$ will be replaced by the n model-conditioned forward-time filtered means and covariances $\left\{ \mathbf{m}_k^i \mid \mathbf{P}_k^i \right\}_{r=1}^n$. It follows then that the likelihoods can be evaluated as

$$\Lambda_k^{ji} = N(\Delta_k^{ji} \mid \mathbf{0}, D_k^{ji}), \tag{41}$$

where

$$\Delta_k^{ji} = \hat{\mathbf{m}}_k^{b,i} - \mathbf{m}_k^j, \tag{42}$$

$$D_k^{ji} = \hat{\mathbf{P}}_k^{b,i} + \mathbf{P}_k^j, \tag{43}$$

The terms d_j can now be computed as

$$d_j = \sum_{i=1}^n p_{ji} \Lambda_k^{ji} \tag{44}$$

The smoothing distribution of the state matched to the models M_k^j and M_{k+1}^j over two successive sampling periods can be expressed as

$$p(\mathbf{x}_k^j \mid M_{k+1}^j, \mathbf{y}_{1:N}) = \frac{1}{c} p(\mathbf{y}_{k+1:N} \mid M_{k+1}^j, \mathbf{x}_k^j) p(\mathbf{x}_k^j \mid \mathbf{y}_{1:k}), \tag{45}$$

where $p(\mathbf{y}_{k+1:N} \mid M_{k+1}^j, \mathbf{x}_k^j)$ is the forward-time model-conditioned filtering distribution, $p(\mathbf{x}_k^j \mid \mathbf{y}_{1:k})$ the backward-time one-step predictive distribution and c a normalising constant.

Thus, the smoothing distribution can be expressed as

$$p(\mathbf{x}_k^j \mid \mathbf{M}_{k+1}^i, \mathbf{y}_{1:N}) (\mathbf{x}_k \mid \hat{\mathbf{m}}_k^{b,i}, \hat{\mathbf{P}}_k^{b,i}) \cdot N(\mathbf{x}_k \mid \mathbf{m}_k^i, \mathbf{P}_k^i), \quad \dots(46)$$

$$= N(\mathbf{x}_k \mid \mathbf{m}_k^{s,ji}, \mathbf{P}_k^{s,ji}), \quad \dots(47)$$

where

$$\mathbf{m}_k^{s,ji} = \mathbf{P}_k^{s,ji} \left[(\mathbf{P}_k^i)^{-1} \mathbf{m}_k^i + (\hat{\mathbf{P}}_k^{b,i})^{-1} \hat{\mathbf{m}}_k^{b,i} \right], \quad \dots(48)$$

$$\mathbf{P}_k^{s,ji} = \left[(\mathbf{P}_k^i)^{-1} + (\hat{\mathbf{P}}_k^{b,i})^{-1} \right]^{-1} \quad \dots(49)$$

The model-conditioned smoothing distributions $p(\mathbf{x}_k^j \mid \mathbf{y}_{1:N})$, which were expressed as mixtures of Gaussians in (36), are now approximated by a single Gaussians via moment matching to yield

$$p(\mathbf{x}_k^j \mid \mathbf{y}_{1:N}) \approx N(\mathbf{x}_k^j \mid \mathbf{m}_k^{s,j}, \mathbf{P}_k^{s,j}), \quad \dots(50)$$

where

$$\mathbf{m}_k^{s,j} = \sum_{i=1}^n \mu_{k+1}^{s,i|j} \mathbf{m}_k^{s,ji}, \quad \dots(51)$$

$$\mathbf{P}_k^{s,j} = \sum_{i=1}^n \mu_{k+1}^{s,i|j} \cdot \left[\mathbf{P}_k^{s,ij} + (\mathbf{m}_k^{s,ij} - \mathbf{m}_k^{s,j})(\mathbf{m}_k^{s,ij} - \mathbf{m}_k^{s,j})^T \right] \quad \dots(52)$$

With these, we can match the moments of the overall smoothing distribution to give a single Gaussian approximation

$$p(\mathbf{x}_k \mid \mathbf{y}_{1:N}) \approx N(\mathbf{x}_k \mid \mathbf{m}_k^s, \mathbf{P}_k^s), \quad \dots(53)$$

where

$$\mathbf{m}_k^s = \sum_{j=1}^n \mu_k^{s,j} \mathbf{m}_k^{s,j}, \quad \dots(54)$$

$$\mathbf{P}_k^s = \sum_{j=1}^n \mu_k^{s,j} \cdot \left[\mathbf{P}_k^{s,j} + (\mathbf{m}_k^{s,j} - \mathbf{m}_k^s)(\mathbf{m}_k^{s,j} - \mathbf{m}_k^s)^T \right] \quad \dots(55)$$

2.4 Model probability estimation and feature extraction

The feature extraction could be applied with the filtered results and smoothed results separately. Based on the filtered results that exist at the same time k , the model M^i with the highest probability μ_k^i is selected as the target motion mode I_k at the moment, which is recorded as

$$I_k = \{I \mid \mu_k^I = \max(\mu_k^i, i = 1, \dots, n)\} \quad \dots(56)$$

The estimation value F of the conversion frequency of target motion model is computed with

$$F = \frac{1}{n} \sum_{i=1}^n \text{var}\{\mu_k^i | k = 1, 2, \dots, T\}, \quad \dots(57)$$

which is the estimation of the motion pattern of a target at successive T time steps measured by the mean variance $\text{var}\{\cdot\}$ of the occurrence probability μ_k^i of n models.

Based on the smoothed results, the smoothed occurrence probability $\mu_k^{s,j}$ is used to replace μ_k^i , so the smoothed estimation value F^s of the conversion frequency of target motion model is obtained.

The manoeuvrability of the flying bird target is usually higher than that of the light and small UAV. If the estimation value of conversion frequency is higher than the threshold S , it is the flying bird target, otherwise, it is the light and small UAV target.

3.0 SIMULATION DATA ANALYSIS

In this section, the effectiveness of the proposed algorithm is evaluated by Monte Carlo experiments on the simulation data of UAV and bird targets. The evaluation methods include the estimation probability, detection rate (P_d), false alarm rate (P_{fa}), root mean square error (RMSE) and receiver operator characteristic (ROC) of different models.

3.1 Simulated model

In this paper, two kinds of simulation models of uniform linear motion and manoeuvring variable speed motion are established. The target of UAV is simulated by uniform linear motion model, and the bird motion is simulated by uniform linear motion model and manoeuvring variable speed motion model.

For the uniform linear motion, the state at the time k includes the target position and velocity, which is expressed as

$$\mathbf{x}_k = (x_k \quad y_k \quad \dot{x}_k \quad \dot{y}_k) \quad \dots(58)$$

The target dynamic model is expressed as

$$\mathbf{x}_{k+1} = \begin{pmatrix} 1 & 0 & \Delta t & 0 \\ 0 & 1 & 0 & \Delta t \\ 0 & 0 & 1 & 0 \\ 0 & 0 & 0 & 1 \end{pmatrix} \mathbf{x}_k + \mathbf{q}_k, \quad \dots(59)$$

where Δt is the data update interval for the system, \mathbf{q}_k is Gaussian process noise with zero mean, and the covariance is

$$E[\mathbf{q}_k \mathbf{q}_k^T] = \begin{pmatrix} \frac{1}{3}\Delta t^3 & 0 & \frac{1}{2}\Delta t^2 & 0 \\ 0 & \frac{1}{3}\Delta t^3 & 0 & \frac{1}{2}\Delta t^2 \\ \frac{1}{2}\Delta t^2 & 0 & \Delta t & 0 \\ 0 & \frac{1}{2}\Delta t^2 & 0 & \Delta t \end{pmatrix} q, \quad \dots(60)$$

where q is the spectral density of noise.

For manoeuvring variable speed motion, the acceleration state variables are also considered as well as the target position and speed. Therefore, the state of the moving target can be represented by

$$\mathbf{x}_k = (x_k, y_k, \dot{x}_k, \dot{y}_k, \ddot{x}_k, \ddot{y}_k) \dots(61)$$

The target dynamic model is expressed as

$$\mathbf{x}_{k+1} = \begin{pmatrix} 1 & 0 & \Delta t & 0 & \frac{1}{2}\Delta t^2 & 0 \\ 0 & 1 & 0 & \Delta t & 0 & \frac{1}{2}\Delta t^2 \\ 0 & 0 & 1 & 0 & \Delta t & 0 \\ 0 & 0 & 0 & 1 & 0 & \Delta t \\ 0 & 0 & 0 & 0 & 1 & 0 \\ 0 & 0 & 0 & 0 & 0 & 1 \end{pmatrix} \mathbf{x}_k + \mathbf{q}_k, \dots(62)$$

where Δt is the data update interval for the system, \mathbf{q}_k is Gaussian process noise with zero mean, and the covariance is

$$E[\mathbf{q}_k \mathbf{q}_k^T] = \begin{pmatrix} \frac{1}{20}\Delta t^5 & 0 & \frac{1}{8}\Delta t^4 & 0 & \frac{1}{6}\Delta t^3 & 0 \\ 0 & \frac{1}{20}\Delta t^5 & 0 & \frac{1}{8}\Delta t^4 & 0 & \frac{1}{6}\Delta t^3 \\ \frac{1}{8}\Delta t^4 & 0 & \frac{1}{6}\Delta t^3 & 0 & \frac{1}{2}\Delta t^2 & 0 \\ 0 & \frac{1}{8}\Delta t^4 & 0 & \frac{1}{6}\Delta t^3 & 0 & \frac{1}{2}\Delta t^2 \\ \frac{1}{6}\Delta t^3 & 0 & \frac{1}{2}\Delta t^2 & 0 & \Delta t & 0 \\ 0 & \frac{1}{2}\Delta t^3 & 0 & \frac{1}{2}\Delta t^2 & 0 & \Delta t \end{pmatrix} q, \dots(63)$$

where q is the spectral density of noise.

In this paper, the time step of the two motion models is set to $\Delta t=0.1$, and the power spectral density of process noise is set to $q=0.1$. The trajectories of all UAVs and flying bird targets are distributed randomly in the space of $[-100,100] \times [-100,100]$, as shown in Fig. 2, including the global view and the partial enlargement of a bird's target trajectory.

The parameters of UAV and flying bird target motion model are set as follows:

1. The UAV target starts randomly in the space of $[-100,100] \times [-100,100]$, with the starting speed amplitude of 3.6 and 240 steps of simulation.

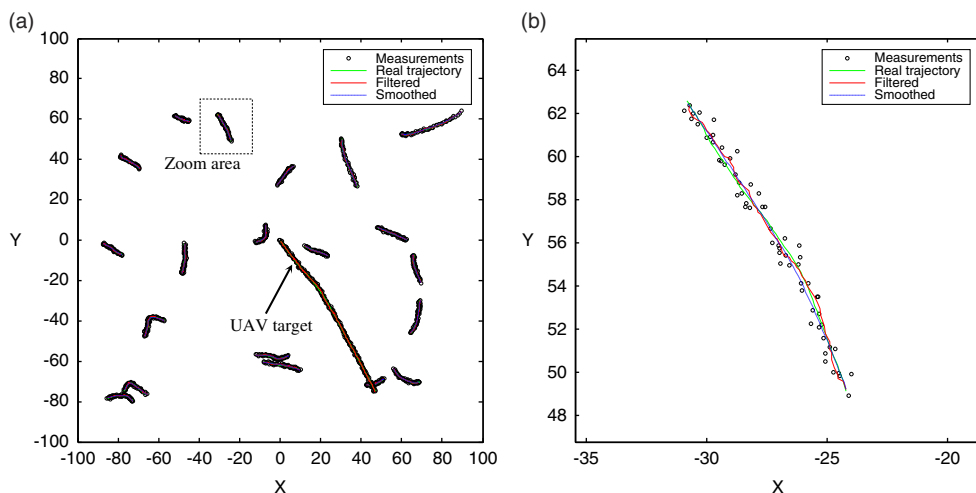


Figure 2. Simulated trajectories of UAV and flying bird targets.

2. The starting point of each bird's target trajectory are distributed randomly in the space of $[-100,100] \times [-100,100]$.
3. The initial velocity amplitude of each bird target is 2, and the initial direction is randomly generated in the range of 0° – 360° .
4. The number of simulation steps of each bird target trajectory is randomly generated in the range of 20–60.
5. The moving model of the flying bird is switched between the uniform linear motion model and the manoeuvring variable motion model, and the switching frequency is controlled by p , which is to generate random numbers between 0 and 1, and when it is less than p , it will switch the motion model once.
6. The UAV and the flying bird target trajectories are all generated by 1,000 times of Monte Carlo simulations.

3.2 Simulation results

Based on the Monte Carlo simulation data of UAV and bird trajectory, the target recognition effect of this algorithm is analysed and verified.

Figure 3 compares the RMSE of UAV and bird target tracking by one Monte Carlo experiment. It is clear that the smoothed algorithm significantly reduce the RMSE of the tracking results for both targets. Table 1 provides a more accurate quantitative comparison by the mean value of 1,000 Monte Carlo experiments, where N represents the number of time steps.

With the increase in the number of time steps, the RMSE of the UAV filtered results is reduced while that of the bird filtered results is increased. For the smoothed results, the RMSE of UAV and bird tracking results both decrease with the increase of simulation steps. The tracking result of UAV is better than that of flying birds due to its smoother flight path. From the comparison data, it can be seen that if the general filter tracking algorithm is used, for more manoeuvrable targets such as birds, more simulation steps often lead to worse tracking results. As for the smoothing algorithm, more simulation steps will improve the tracking results for different manoeuvring targets such as birds and UAVs.

Figures 4 and 5 show the model probability estimation results in a certain tracking simulation of UAV and flying bird target, respectively, in which the model switching frequency of flying bird target is $p = 0.3$. In the 240-step tracking simulation of UAV target, the filtering estimation probabilities of models 1 and 2 are about 0.8 and 0.2, respectively, and the smoothed estimation probabilities are close to 1 and 0, which indicates that the uniform linear motion model is used only. In the 60-step tracking simulation of bird, the target is switched

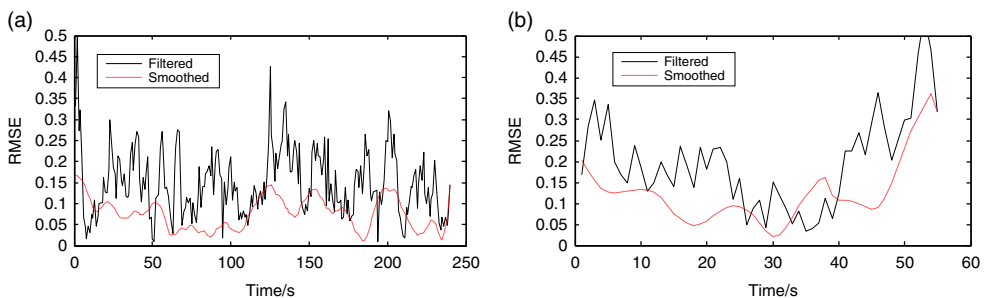


Figure 3. RMSE of target tracking.

Table 1
RMSE of simulated target tracking by 1,000 Monte Carlo experiments

N	Target	RMSE	
		Filtered	Smoothed
50	UAV	0.1645	0.0922
	Bird	0.2143	0.1198
100	UAV	0.1595	0.0831
	Bird	0.2188	0.1175
150	UAV	0.1567	0.0803
	Bird	0.2210	0.1160
200	UAV	0.1556	0.0789
	Bird	0.2220	0.1158

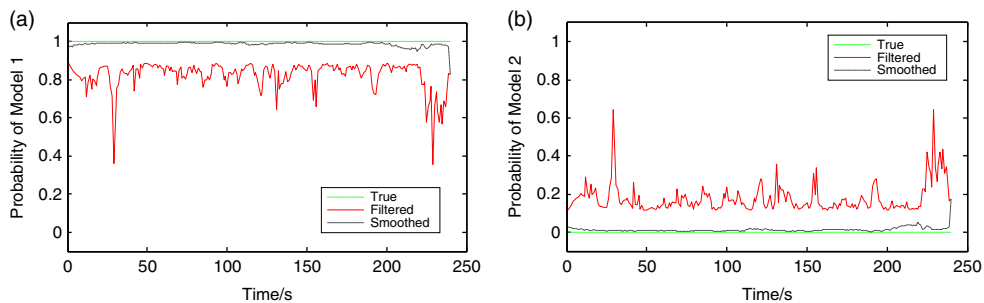


Figure 4. Estimation of model probability in the tracking of UAV target.

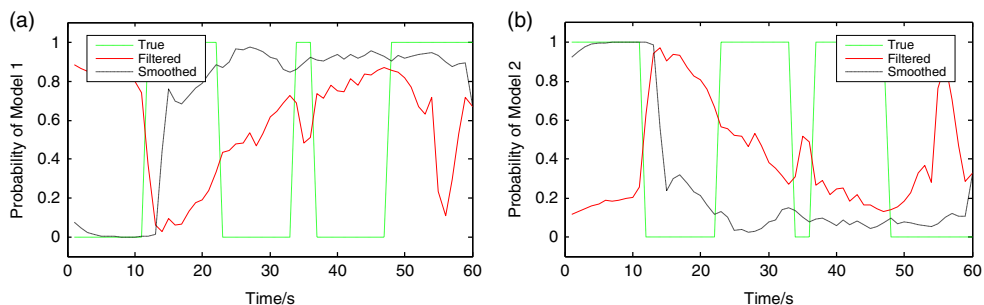


Figure 5. Estimation of model probability in the tracking of flying bird target.

five times between models 1 and 2, and the filtered and smoothed estimation probability of the two models both fluctuates greatly, obviously higher than that of UAV target, which characteristic could be used to distinguish these two targets.

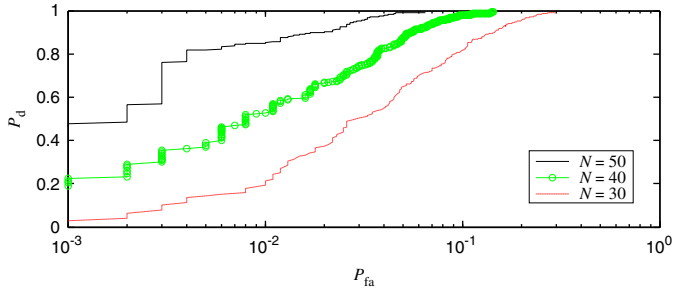


Figure 6. ROC curves with the filtering algorithm by different number of recognition steps.

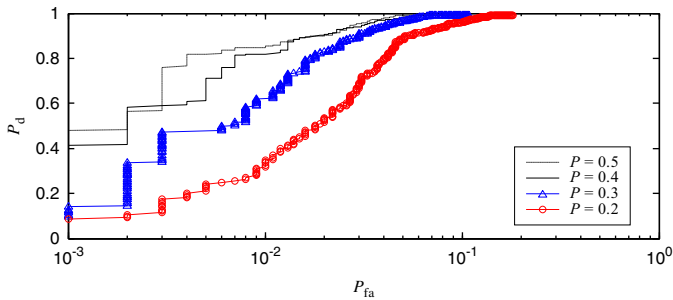


Figure 7. ROC curves with the filtering algorithm under different probabilities of model change.

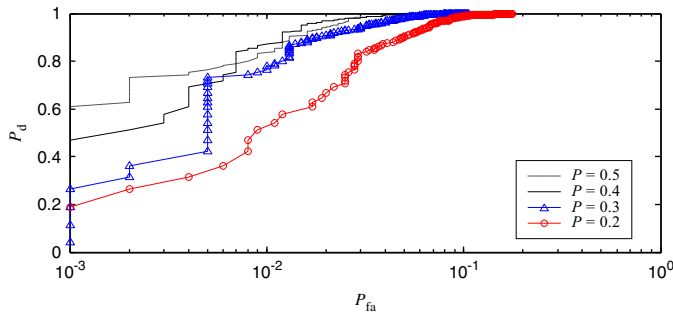


Figure 8. ROC curves with the smoothing algorithm under different probabilities of model change.

Figures 6–9 show the ROC curves based on 1,000 Monte Carlo simulation data under different parameters, where the UAV is the target and the bird is the false alarm.

Figure 6 shows the ROC curves with the filtering algorithm by different number of recognition steps N . It can be seen that more steps led to better recognition effect. The reason is simple that the more recognition steps, the more obvious the stability of the UAV flight path and the manoeuvrability of the flying bird target be exposed, so it is naturally easier to identify.

Figures 7 and 8 show the ROC curves with the filtering and smoothing algorithm under different probabilities of model change. The number of recognition steps is set to $N=50$. The larger the p value, the higher the transformation frequency of the bird target motion model is,

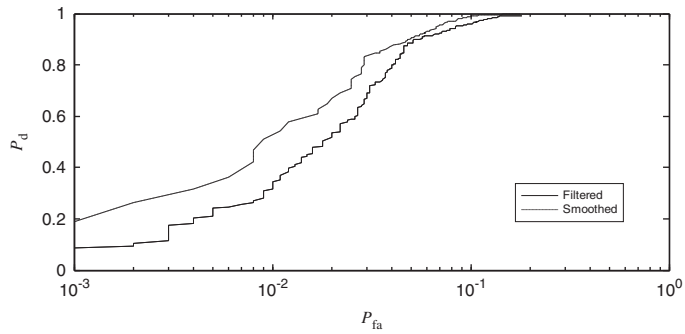


Figure 9. Comparison of the ROC curves between the filtered and smoothed algorithm.



Figure 10. Surveillance radar at airport.

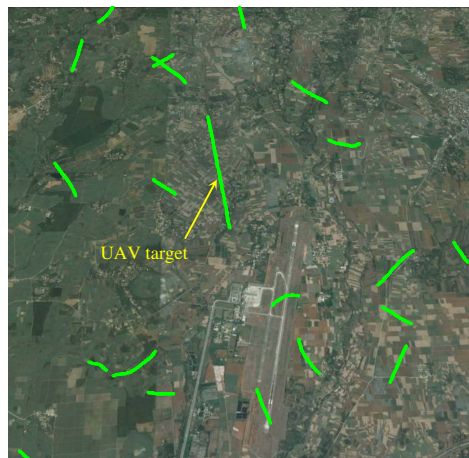


Figure 11. Radar surveillance data at airport.

the easier it is to identify it. As can be seen from the figures, the false alarm rate for flying birds is less than 15% when the detection rate of UAV target is close to 100%, regardless of filtering or smoothing algorithm.

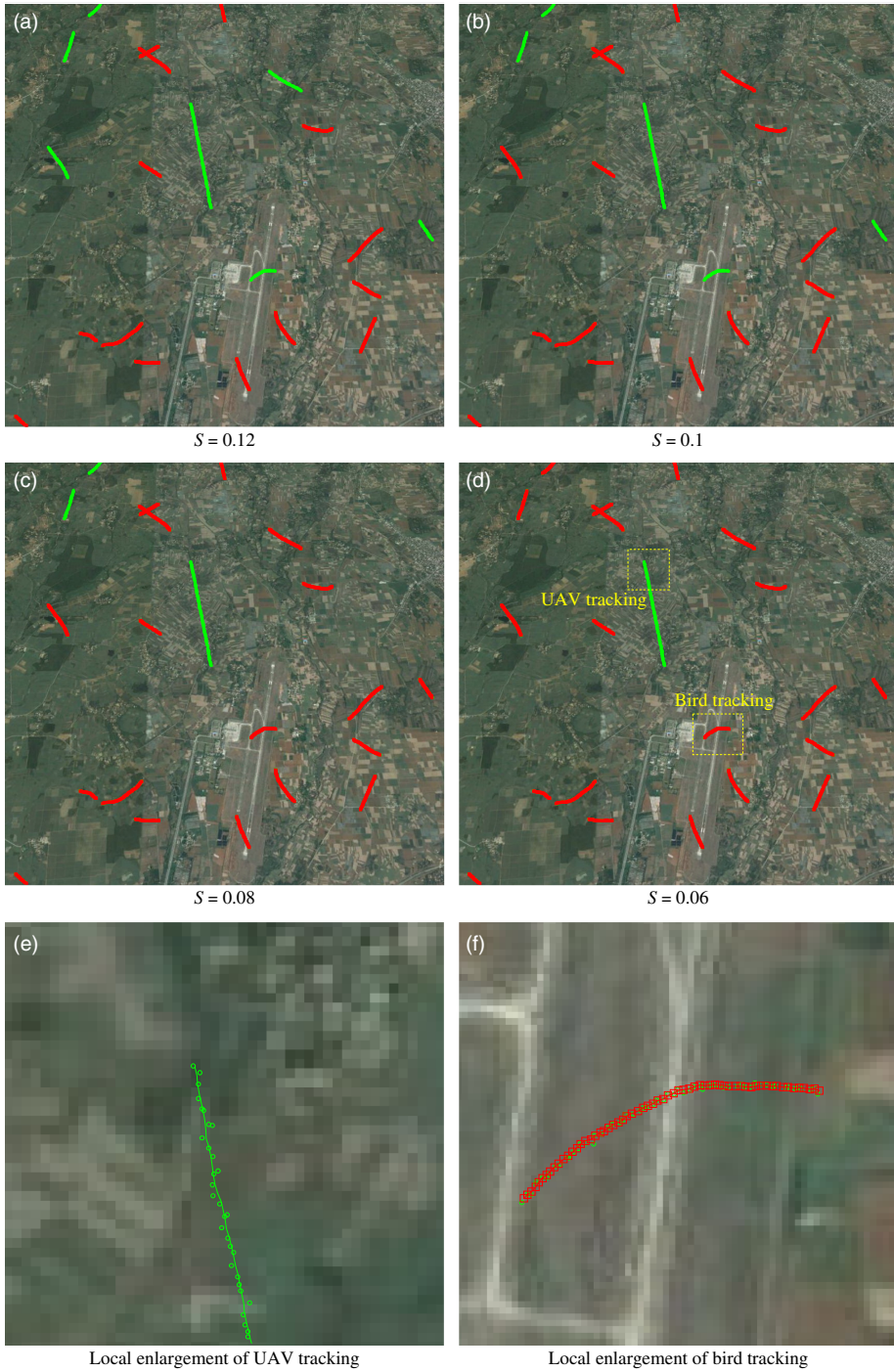


Figure 12. Classification of UAV and bird targets with case 1.

Figure 9 gives the comparison of the ROC curves between the filtered and smoothed algorithm with the parameter $p=0.2$. Compared with the filtering algorithm, the smoothing algorithm enlarges the gap between the estimations of target model conversion frequency for the flying bird and UAV, improving the accuracy of target recognition.

4.0 REAL DATA ANALYSIS

Based on the low-altitude radar surveillance system installed at airport and coastal area, a large number of radar data containing UAVs and flying birds have been collected, and the previous research has realised the detection and tracking of all kinds of targets^(1,17–20). This section will process and analyse the radar data collected from the above two outfields.

4.1 Case 1

An example of airport application is given in this section. Figure 10 shows a radar system installed on the roof of an airport light station. Figure 11 is the radar measurements collected at a certain period of time with the coverage radius of 5km. The measured data are overlaid on the satellite map and expressed by ‘°’, which includes a test UAV of DJI Phantom series and some flying birds in the natural environment of the airport. The flying birds in the radar data shown in Fig. 11 are mostly local resident birds in the foraging state, with short flying distance and high manoeuvrability. The proposed algorithm is used to track and classify the UAV and flying bird targets. The number of recognition steps is set to $N=50$.

In engineering applications, first, the UAV and bird targets are identified by artificial methods, and the model transformation probability estimates of different targets are calculated, then the classification thresholds of UAV and bird targets are set. In different test environments, the thresholds are often different and need to be measured by experimental methods to ensure the recognition effect of the system. Figure 12 shows the tracking and recognition results of UAV and bird targets under different thresholds, and the local enlargement drawings. The UAV trajectory is represented by a solid line and the bird trajectory is represented by ‘□’. When the threshold is high, some flying birds are mistaken for UAV. Only when the threshold is low enough (Fig. 12(d), $S=0.06$) can all the flying birds be

Table 2
Recognition results of UAV and bird targets for case 1

S	UAV	Bird
0.04	1	20
0.06	1	20
0.08	3	18
0.10	5	16
0.12	6	15
0.14	12	9
0.16	17	4

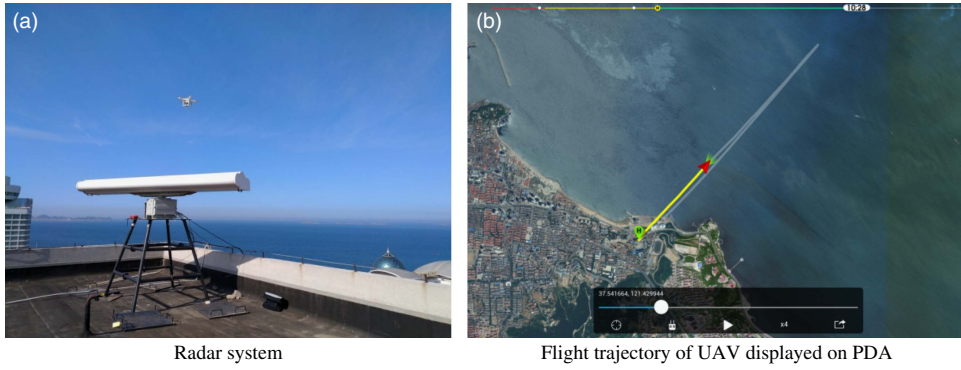


Figure 13. Surveillance radar at coastal area.

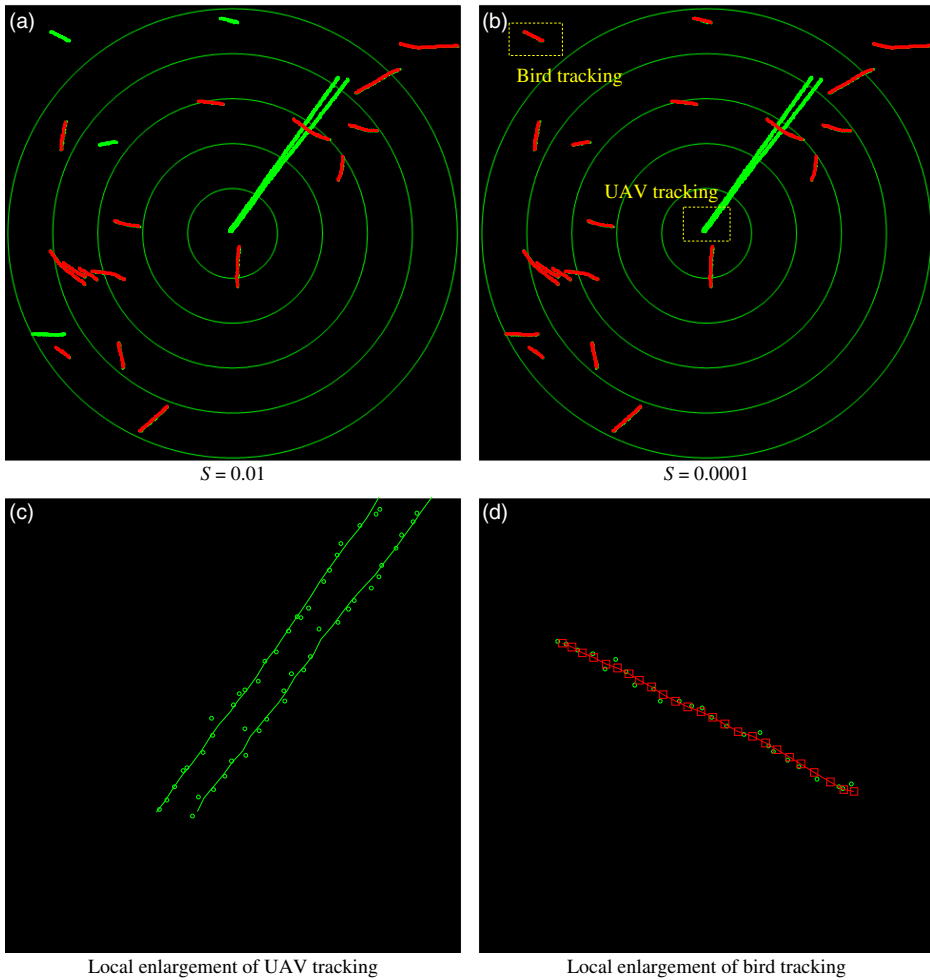


Figure 14. Classification of UAV and bird targets with case 2.

Table 3
Recognition results of UAV and bird targets
for case 2

<i>S</i>	UAV	Bird
0.0001	1	20
0.001	2	19
0.01	5	16
0.05	5	16
0.1	8	13
0.12	8	13
0.14	12	9
0.16	15	6
0.18	17	4

recognised correctly. Referring to Fig. 12, Table 2 shows the quantitative identification results under different thresholds.

4.2 Case 2

An example of coastal application is given in this section. Figure 13 shows a radar system installed on high-rise buildings near the coast and the flight trajectory of UAV displayed on personal digital assistant (PDA). The test UAV target flew back and forth, reaching the longest distance of 3 km. In addition to UAV, the targets in radar data are mostly coastal waterfowls. Figure 14 and Table 3 give the classification results of UAV and bird targets with case 2. The difference between this case and the above one is that in this case, the flying mode of waterfowl over the sea is mostly gliding, whose manoeuvrability is slightly lower and closer to that of UAVs. Therefore, only when the threshold is set low enough (Fig. 14(b), $S=0.0001$) can the birds and UAVs in radar data be distinguished completely right.

5.0 CONCLUSIONS

In this paper, a classification and recognition method of light and small UAV and flying bird targets is proposed, which is based on the non-co-operative target information obtained by conventional low-altitude radar and is characterised by the conversion frequency of target motion model. The effectiveness of the algorithm is verified by simulation and radar data, and the following conclusions are drawn:

- This algorithm is suitable for conventional mechanical scanning surveillance radar data and can distinguish UAV and flying bird target by using less echo information such as moving direction, velocity and position of the target.
- According to the simulation data, the variance mean of the estimated frequency of UAV target motion model conversion is more than one order of magnitude lower than that of the bird target with high manoeuvrability.
- The smoothing algorithm enlarges the gap between the estimations of target model conversion frequency for the flying bird and UAV, outperforming the filtering algorithm in target recognition accuracy.

- (d) For some flying birds with low manoeuvrability, the moving mode is similar to that of UAV, and the false alarm is easy to be caused by the proposed algorithm. It is necessary to recognise and classify the flying birds with other refined processing techniques such as target micro-Doppler characteristics.
- (e) The micro-Doppler characteristics of the target reflect the inherent motion properties of the target to a certain extent and are closely related to the structure of the target and the electromagnetic scattering characteristics. Therefore, with the gradual improvement of the detection performance of low-altitude surveillance radar, micro-Doppler characteristics will become an important means and way for the detection and recognition of LSS targets such as UAVs.

ACKNOWLEDGEMENTS

The research work is jointly funded by the National Natural Science Foundation of China (NSFC) and Civil Aviation Administration of China (CAAC) (U1633122) and supported by the National Key Research and Development Program (2016YFC0800406).

REFERENCES

1. CHEN, W.S. The supervision, detection and jamming technologies for light and small UAV, *China Civil Aviation*, 2017, **253**, (7), pp 33–34.
2. LV, X.M. Military UAV development and countermeasures, *National Defense Sci and Technology*, 2013, **34**, (1), pp 5–7.
3. CHEN, C.S. and WANG, S.Y. Infrared radiation characteristics measurement and temperature retrieval based on DJI unmanned aerial vehicle, *Opto-Electronic Engineering*, 2017, **44**, (4), pp 427–434.
4. ROHDE and SCHWARZ. Automatic identification, positioning and suppression system of UAV (I), *China Radio*, 2016, **23**, (8), pp 72–73.
5. ROHDE and SCHWARZ. Automatic identification, positioning and suppression system of UAV (II), *China Radio*, 2016, **23**, (9), pp 71–72.
6. ROHDE and SCHWARZ. Automatic identification, positioning and suppression system of UAV (III), *China Radio*, 2016, **23**, (10), pp 72–73.
7. LV, B., WANG, A.J., MA, Y. and ZHOU, Y.Z. Radio technology application in civil UAV control, *China Radio*, 2017, **8**, pp 24–26.
8. CHEN, W.S., YAN, J. and LI, J. Joint optimization of detection and tracking with Rao-Blackwellized Monte Carlo data association, *J Beijing University of Aeronautics and Astronautics*, 2018, **44**, (4), pp 700–708.
9. CHEN, X.L., GUAN, J., HUANG, Y. and HE, Y. Radar low-observable target detection, *Science & Technology Review*, 2017, **35**, (11), pp 30–38.
10. CHEN, X.L., GUAN, J., HUANG, Y., YU, X.H., LIU, N.B., DONG, Y.L. and HE, Y. Radar refined processing and its applications for low-observable moving target, *Sci and Technology Review*, 2017, **35**, (20), pp 19–27.
11. ZHANG, J., XU, Q.Y., CAO, X.B., YAN, P.K. and LI, X.L. Hierarchical incorporation of shape and shape dynamics for flying bird detection, *Neurocomputing*, 2014, **131**, (5), pp 179–190.
12. BAI, X.R., XING, M.D., ZHOU, F., LU, G.Y. and BAO, Z. Imaging micromotion targets with rotating parts based on empirical-mode decomposition, *IEEE Transactions on Geoscience and Remote Sensing*, 2008, **46**, (11), pp 3514–3523.
13. STANKOVIC, L., THAYAPARAN, T., DAKOVIC, M. and POPOVIC-BUGARIN, V. Micro-Doppler removal in the radar imaging analysis, *IEEE Transactions on Aerospace and Electronic Systems*, 2013, **49**, (2), pp 1234–1250.
14. ZHANG, Q., YEO, T.S., TAN, H.S. and LUO, Y. Imaging of a moving target with rotating parts based on the Hough transform, *IEEE Transactions on Geoscience and Remote Sensing*, 2008, **46**, (1), pp 291–299.

15. ZHANG, Q., HE, Q.F. and LUO, Y. Micro-Doppler feature extraction of group targets using signal decomposition based on Bessel function basis, *J Electronics and Information Technology*, 2016, **38**, (12), pp 3056–3062.
16. ZHANG, Q. and LUO, Y. *Micro-Doppler Effect of Radar Targets*, National Defense Industry Press, 2013, Beijing, PRC.
17. CHEN, W.S. and LI, J. Radar target detection in low-altitude airspace with spatial features, *Acta Aeronautica et Astronautica Sinica*, 2015, **36**, (9), pp 3060–3068.
18. CHEN, W.S. Incoherent radar target detection and tracking with temporal features, *Systems Engineering and Electronics*, 2016, **38**, (8), pp 1800–1807.
19. CHEN, W.S. Spatial and temporal features selection for low-altitude target detection, *Aerospace Sci and Technology*, 2015, **40**, (1), pp 171–180.
20. CHEN, W.S. and LI, J. Review on developments and applications of avian radar technology, *Modern Radar*, 2017, **39**, (2), pp 7–17.